PTEP

Prog. Theor. Exp. Phys. **2018**, 103D02 (20 pages)
DOI: 10.1093/ptep/pty107

Signature of yrast-state structure in even–even hafnium isotopes based on traditional total-Routhian-surface calculations and novel E-GOS curves

Hai-Yan Meng[1], Yi-Wei Hao[1], Hua-Lei Wang[1,*], and Min-Liang Liu[2]

[1]*School of Physics and Engineering, Zhengzhou University, Zhengzhou 450001, China*
[2]*Institute of Modern Physics, Chinese Academy of Sciences, Lanzhou 730000, China*
[*]E-mail: wanghualei@zzu.edu.cn

Received June 5, 2018; Revised September 7, 2018; Accepted September 13, 2018; Published October 31, 2018

The yrast properties, including quadrupole deformation β_2, moment of inertia, and collective mode, have been systematically investigated in macroscopic–microscopic frameworks in terms of pairing self-consistent Woods–Saxon–Strutinsky calculations (e.g., the total-Routhian-surface method) for even–even Hf isotopic mass chains. The calculated results indicate that the equilibrium deformations are model- and parameter-dependent, especially for soft nuclei. Deformation Routhian curves are presented to display the shape and softness evolution. The backbending or upbending behavior in the moment of inertia is attributed to band-crossing of high-j orbitals, generally corresponding to neutron $i_{13/2}$ or proton $h_{11/2}$ ones here. It is found that some nuclei in this region have relatively complicated yrast components (e.g., prolate or oblate 0-, 2-, or 4-quasiparticle bands, even non-collective excitations, etc.) with rotation due to a high band density (namely, the appearance of many bands with a narrow energy domain for a given spin). The reason of the simultaneous rise in neutron and proton aligned angular momenta might be a shape jump rather than the traditional physics scenario of the competition between the neutron and proton alignments, e.g., in the heavier $^{180-184}$Hf. Besides these, the evolution between different collective motion modes (such as rotational, γ-soft, and vibrational ones) along the yrast line is briefly investigated using our developed centipede-like E-GOS (E-gamma over spin) curve. Moreover, taking this isotopic chain as a carrier, a further extended E-GOS curve is given by including the first-order rotation–vibration interaction, showing an apparent improvement in the predictive power of motion evolution and the necessity of the inclusion of such a coupling in future theoretical work, even for well deformed nuclei.

Subject Index D11, D12, D13

1. Introduction

Thanks to important technological developments in the production and exploitation of nuclei far from stability (namely, so-called exotic nuclei), in the development of more powerful instruments (such as heavy-ion accelerators, radioactive beam facilities, highly effective detector arrays and those for the selection of nuclei produced in heavy-ion reactions and for their spectroscopy, or of trapping devices and storage rings for mass measurements), and in the capacity of modern computers to collect and handle such data, it is possible to observe individual levels up to rather high spins in many nuclei, which provide researchers with a good opportunity to systematically investigate the evolution of nuclear intrinsic structure along a specific "pathway" (such as an isotopic or isotonic chain, angular

momentum, excitation energy, etc.). Indeed, related studies have revealed numerous interesting phenomena such as unexpected onsets of collectivity, shell-gap modifications, backbending, and shape/phase transition [1–4].

Theoretically, as a final goal, the derivation of nuclear structure from the interactions of quarks and gluons is, in principle, expected. However, in order to make the task tractable and more physically intuitive, in practice, a number of simplifications in theoretical modeling usually have to be made. For instance, the use of the concept of nucleons and their interactions in nuclei is the first approximation that has been adopted in nearly all current nuclear models including ab initio, self-consistent mean-field, and macroscopic–microscopic approaches [5]. Even the so-called ab initio methods are attempting to derive nuclear properties based on the free interactions of their constituent nucleons [6,7]. Indeed, electron scattering experiments and related calculations have to a large extent confirmed that such an approximation of treating nuclei in terms of nucleons can work well down to surprisingly small distance scales of about 0.5 fm, and that the quark–gluon-based description is more appropriate at the level of 0.1 fm or so [8,9]. Nevertheless, due to the difficulty of solving the many-body problem, another simplification, namely, the mean-field approximation including phenomenological or empirical and self-consistent methods, is usually made, especially for heavier nuclei, which assumes that all the nucleons conspire to create a single potential in which they independently move along their orbits. Nowadays, based on the basic framework of Hartree or Hartree–Fock theory and different nucleon–nucleon interactions, various self-consistent mean-field approaches have been developed, such as the Skyrme–Hartree–Fock model [10], the Gogny Hartree–Fock–Bogoliubov model [11], and even the relativistic mean-field model [12,13] with nucleons, hyperons, and mesons.

However, empirical one-body mean-field potentials, like the Woods–Saxon and Nilsson ones, are still widely used and frequently developed to study nuclear properties by combining a macroscopic bulk part (e.g., a standard liquid model [14], a finite-range droplet model [15], and the Lublin–Strasbourg drop model [16]) due to the double-counting effect. Such macroscopic–microscopic methods usually have very high descriptive power as well as simplicity of calculation, and such one-body potentials corresponding to nuclear shape can generally be described by the multipole expansion of a nuclear surface with spherical harmonics [17,18], which will be very suitable for studying nuclear intrinsic symmetries. Moreover, taking the cranking approximation (e.g., introduced by Inglis [19,20]) into account, one can reveal nuclear properties under rotation, especially along the yrast line. As one of the most significant fields in nuclear structure, the yrast level and its structure, which also play a crucial role in deciding the course and outcome of many nuclear reactions [21], have attracted considerable attention. In the present work, we will systematically investigate the intrinsic structure and its evolution along the yrast line in even–even nuclei of the hafnium isotopic chain. As is known, the ground state with zero angular momentum in even–even nuclei is typically a superconducting state with paired nucleons moving in orbits, while the yrast state means the state with lowest energy at a given angular momentum. Therefore, to understand the yrast property, one has to answer how angular momentum can be generated in nuclei with the lowest energy expenditure. In the hafnium isotopes, most nuclei are deformed and it is, of course, expected that collective rotation will be energetically the most favorable mode to produce spin. However, it is interesting to enquire whether the yrast structure will remain in the ground-state band, or develop into decoupled 2-quasiparticle (even multi-quasiparticle) bands or something else, whether vibration or few-particle degrees of freedom can be a competitive mode, and whether the different motion modes can couple to some extent.

With these questions in mind, we perform pairing-deformation self-consistent Woods–Saxon–Strutinsky calculations within the framework of the macroscopic–microscopic model and cranking approximation [22] for even–even $^{156-184}$Hf nuclei in which at least three yrast excited states are observed experimentally, focusing on band-crossings, phase/shape transitions, nuclear softnesses, motion modes, and the reliability when extrapolating the model into high-isospin (proton or neutron drip-line) and/or high-spin regions. So far, 36 hafnium members from $A = 154$ to 189, including 6 stable (^{174}Hf and $^{176-180}$Hf), 21 proton-rich, and 9 neutron-rich isotopes, have been discovered in this hafnium isotopic chain by mainly using different reaction techniques such as heavy-ion fusion evaporation, light-particle reactions, projectile fragmentation, or deep inelastic reactions combined with sensitive γ-ray spectrometers [23]. Moreover, it is predicted in terms of the HFB-14 mass model [24] that the last odd–even and even–even particle stable neutron-rich nuclei will respectively be ^{235}Hf and ^{240}Hf [23]. On the neutron-deficient side, at least 4 nuclei $^{150-153}$Hf may be particle stable and even 7 more nuclei $^{143-149}$Hf could possibly have half-lives longer than 10^{-9} s [25], indicating that such nuclei may be accessed experimentally. Indeed, the proton-emitting nucleus ^{153}Hf was produced by using projectile fragmentation of a very heavy beam of ^{197}Au and a ^{90}Zr target [26]. Thus, there is reason to believe that much more yrast information under extreme conditions of spin and isospin will be frequently revealed and a systematic investigation will extend our knowledge and understanding of nuclear yrast structures.

The remainder of this paper is organized as follows. In Sect. 2, we will outline the unified procedure of the theoretical method and simultaneously provide the necessary references. The results and discussion are presented in Sect. 3. Finally, we give a summary in Sect. 4.

2. Theoretical descriptions

Nuclear energy surface calculations including configuration-constrained potential-energy surface (PES) [27] and total-Routhian-surface (TRS) [28–30] ones are powerful theoretical tools in nuclear structure research. Such models have several standard components such as macroscopic liquid-drop energy, microscopic shell and pairing corrections, and the Coriolis term for the TRS calculation, each one individually familiar from the literature. Here, we will briefly outline the unified procedure and provide the necessary references (note that the theoretical methods can also be seen in our previous work [32–35] and references therein).

In the PES method, the total potential energy $E_{\rm total}(Z,N,\hat{\beta})$ of a nucleus with deformation $\hat{\beta}$ is the sum of a macroscopic bulk-energy term $E_{\rm mac}(Z,N,\hat{\beta})$, being a smooth function of Z,N, and deformation, and a microscopic term $\delta E_{\rm mic}(Z,N,\hat{\beta})$ representing the quantum correction based on some phenomenological single-particle potential [15,27]. The macroscopic energy is obtained from the standard liquid-drop model with the parameters used by Myers and Swiatecki [14]. The microscopic correction part, which arises from the nonuniform distribution of single-particle levels, is calculated by means of the well known Strutinsky approach [29,31,36] whose development has ever been considered as a major leap forward in the nuclear many-body problem. The single-particle energies and the single-particle wave functions are calculated by solving the Schrödinger equation of the stationary states for an average nuclear potential of Woods–Saxon (WS) type [37,38] including a central field, a spin–orbit interaction, and the Coulomb potential for the protons. The universal WS parameter set is adopted, i.e.,

(a) Radius parameters: $r_0(p) = 1.275$ fm, $r_0(n) = 1.347$ fm, $r_{0-so}(p) = 1.320$ fm, $r_{0-so}(n) = 1.310$ fm;

(b) Central potential depth parameters: $V_0 = 49.6$ MeV, $\kappa = 0.86$;
(c) Spin–orbit potential strength constants: $\lambda(p) = 36.0$, $\lambda(n) = 35.0$;
(d) Diffuseness parameters: $a_0(p) = a_0(n) = a_{0-so}(p) = a_{0-so}(n) = 0.70$ fm.

The deformed WS potential is generated numerically in the 3D deformation space $(\beta_2, \gamma, \beta_4)$. To reduce the unphysical fluctuation of the weakened pairing field, an approximate particle-number projection is employed based on the Lipkin–Nogami (LN) approach [29,31] with monopole pairing considered. The monopole pairing strength G is determined by the average gap method [39,40]. The LN equations are solved in a sufficiently large space of WS single-particle states. Finally, the PES will be obtained by interpolating between the selected lattice points in the multidimensional deformation space. The minimum of the PES gives the corresponding nuclear properties, e.g., energy, equilibrium deformations, and pairing gap.

Similar to the PES method, generalized to the case of rotation [41–44], the total Routhian $E^{\omega}(Z, N, \hat{\beta})$ of a nucleus (Z, N) at frequency ω and deformation $\hat{\beta}$, which is called "Routhian" instead of "energy" in a rotating frame of reference, is the sum of the energy of the non-rotating state (the same as the PES calculation) and the contribution due to rotation calculated by the cranking shell model [29]. Note that, under rotation, the nuclear system is here cranked around a fixed axis (e.g., the x-axis) at a given rotational frequency ω. In such a cranking situation, the single-particle levels can be calculated by using a set of new WS parameters (relative to the universal WS parameter set; for convenience, let us temporarily call this the cranking WS parameter set) [45]:

(a) Radius parameters: $r_0(p) = r_0(n) = r_{0-so}(p) = r_{0-so}(n) = 1.190$ fm;
(b) Central potential depth parameters: $V_0 = 53.754$ MeV, $\kappa = 0.791$;
(c) Spin–orbit potential strength constants: $\lambda(p) = \lambda(n) = 29.494$;
(d) Diffuseness parameters: $a_0(p) = a_0(n) = a_{0-so}(p) = a_{0-so}(n) = 0.637$ fm.

Such a parameter set can give a better description of charge radii (both magnitude and isospin dependence) and high-spin properties (e.g., moment of inertia) in nuclei (see Refs. [45,46] and references therein), especially in medium and heavy mass regions. Moreover, besides monopole pairing, doubly stretched quadrupole pairings are considered, which will be important for the proper description of, e.g., the nuclear moment of inertia and backbending frequency, though they have a negligible effect on energy [47]. The quadrupole pairing strengths are calculated by restoring the Galilean invariance broken by the seniority pairing force [48,49]. Pairing correlations depend on rotational frequency and deformation. The resulting cranking LN equation takes the form of the well known Hartree–Fock–Bogolyubov-like (HFB) equation, which can be solved by using the HFB cranking (HFBC) method [22,50]. While solving the HFBC equations, pairing is treated self-consistently at each frequency ω and each grid point in the selected deformation space. After the numerically calculated Routhians at fixed ω are interpolated using a cubic spline function between the lattice points, the equilibrium deformations can be determined by minimizing the calculated TRS. Then, other conserved quantities at such a shape can be solved in principle.

It should be noted that, in the actual calculations, Bohr shape deformation parameters [51] are adopted. Thus, the β_2 value is always positive and the prolate, oblate, and triaxial shapes can be denoted by the γ parameter. To describe the rotational case conveniently, we use the Lund convention [44] of γ values ranging from $-120°$ to $60°$. Such a γ range can be divided into three sectors, $-120° < \gamma < -60°$, $-60° < \gamma < 0°$, and $0° < \gamma < 60°$, which represent the same triaxial shapes in the ground state but respectively represent rotation about the long, intermediate, and short axes at

nonzero cranking frequency. The four limiting values ($-120°$, $-60°$, $0°$, and $60°$) correspond to the possible rotations of axially symmetric shapes ($-120°$ and $0°$ for prolate and $\pm 60°$ for oblate shapes) with various orientations of the nuclear axes with respect to the rotation axis ($\gamma = -120°$ and $60°$ mean that the nucleus rotates around its symmetry axis—non-collective rotation—and $\gamma = -60°$ and $0°$ mean that the nucleus rotates around an axis perpendicular to the symmetry axis—collective rotation).

3. Calculations and discussions

3.1. Total-Routhian-surface calculation

Phenomenological or empirical laws obtained in nuclear structure research are often simple but valid to evaluate the nuclear properties. Figure 1 shows two such phenomenological quantities. For

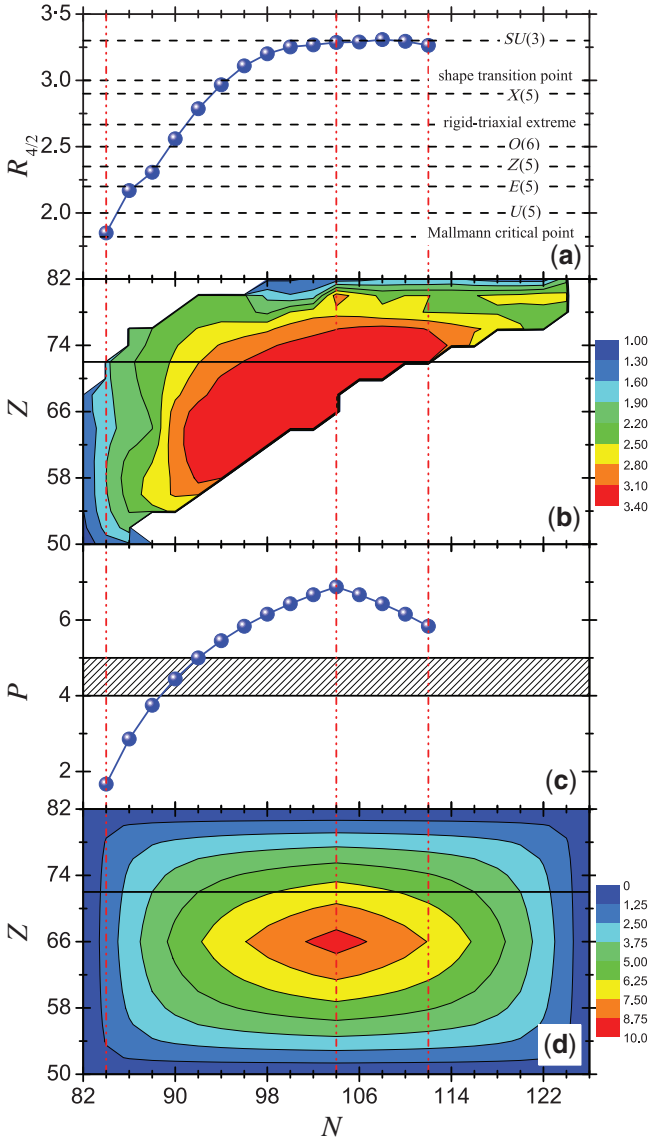

Fig. 1. The available phenomenological ratio $R_{4/2}$ (a) and the P factor (c) for even–even Hf isotopes. Also, the corresponding $R_{4/2}$ contours (b) and the P-factor contours (d) in this region are plotted to provide a helpful understanding of the situation of Hf isotopes. The solid lines in (b) and (d) denote the isotopic positions with $Z = 72$.

Table 1. The calculated results (PES: with universal parameter set; TRS: with cranking parameters) for the ground-state equilibrium deformation parameter β_2 for even–even $^{156-184}$Hf, together with the FY+FRDM [66], HFBCS [67], and ETFSI [68] calculations and partial experimental values (Exp.) [69] for comparison.

Nuclei	PES	TRS	FY+FRDM	HFBCS	ETFSI	Exp.[a]
^{156}Hf	0.060	0.078	0.035	0.000	0.090	–
^{158}Hf	0.118	0.131	0.107	0.000	0.140	–
^{160}Hf	0.154	0.161	0.152	0.140	0.180	–
^{162}Hf	0.180	0.183	0.180	0.190	0.210	0.158
^{164}Hf	0.200	0.203	0.208	0.220	0.250	0.197
^{166}Hf	0.223	0.222	0.226	0.230	0.270	0.250
^{168}Hf	0.243	0.245	0.254	0.270	0.290	0.275
^{170}Hf	0.270	0.284	0.274	0.290	0.310	0.301
^{172}Hf	0.300	0.300	0.284	0.300	0.330	0.276
^{174}Hf	0.283	0.292	0.285	0.320	0.320	0.286
^{176}Hf	0.271	0.272	0.277	0.280	0.320	0.295
^{178}Hf	0.262	0.262	0.278	0.260	0.290	0.280
^{180}Hf	0.255	0.256	0.279	0.220	0.290	0.274
^{182}Hf	0.247	0.249	0.270	0.240	0.280	–
^{184}Hf	0.235	0.238	0.260	0.250	0.260	–

[a]The uncertainties are less than 0.01 except for ^{170}Hf (0.035); see Ref. [69] for details.

instance, the energy ratio of the first 4_1^+ and 2_1^+ excited states in even–even nuclei, namely, $R_{4/2}$ ($\equiv E(4_1^+)/E(2_1^+)$), is generally regarded as a good indicator of different collective motions and critical point symmetries of a nucleus, especially in low-lying nuclear structure. As is well known, based on some ideal assumptions, the energy ratio $R_{4/2}$ has been predicted to be 10/3 for a well deformed axially symmetric rotor, 2.5 for the γ-unstable limit, and 2.0 for a spherical vibrator, corresponding to $SU(3)$, $O(6)$, and $U(5)$ dynamic symmetries, respectively, in the algebraic view of the interacting boson model [52,53]. Further, the $R_{4/2}$ value will be about 2.9 for the $X(5)$ symmetry (the critical point of the spherical to deformed transition path), 2.2 for the $E(5)$ symmetry (the critical point of the spherical to γ-unstable vibrator path), and 2.35 for $Z(5)$ symmetry (the prolate to oblate nuclear shape/phase transition) [54,55]. It has also been pointed out that the $R_{4/2}$ values 1.82, 8/3, and 3.0 respectively correspond to the so-called Mallmann critical point, which is the separatrix between single-particle and collective characteristics [56], the triaxial extreme with $\gamma = 30°$ according to the Davydov–Filippov rigid-triaxial rotor model [57], and the shape/phase transition point to quadrupole deformed nuclei [58,59]. So far, these nine critical $R_{4/2}$ values are widely used to identify collective properties of even–even nuclei. As shown in Fig. 1(a), all the available $R_{4/2}$ values are greater than the Mallmann critical point, undoubtedly indicating the onset of collective characteristics. The $R_{4/2}$ values of the six lighter nuclei $^{156-166}$Hf are smaller than the shape transition point 3.0, in good agreement with the soft energy surfaces as discussed below, and the remaining $^{168-184}$Hf nuclei with $R_{4/2} > 3.0$ show relatively strong collectivity (e.g., large β_2; see Table 1). More precisely, one can also see from Fig. 1(a) that the nine critical points will divide the energy ratio $R_{4/2}$ into ten regions with different collective properties. In the global nuclear chart, all the even–even nuclei with corresponding properties can, in principle, be found and investigated according to these laws of this $R_{4/2}$ ratio. In Fig. 2(b), the contours of the available $R_{4/2}$ data are plotted for the selected region, showing a rather regular $R_{4/2}$ distribution.

Besides the $R_{4/2}$ ratio, another more sensitive phenomenological quantity related to nuclear collectivity and deformation is the P factor [60–64], which is defined by $P \equiv N_p N_n/(N_p + N_n)$, where

N_p and N_n are respectively the numbers of valence protons and neutrons; the product N_pN_n denotes the number of p–n interactions and the summation $N_p + N_n$ means the number of pairing interactions. Thus, this factor can be viewed as the average number of interactions of each valence nucleon with those of the other type. It has been pointed out that nuclear deformation may be explained as being due to competition between the pairing interaction of like nucleons, which has a symmetry-restoring effect, and the neutron–proton interaction, which is responsible for strong mixing of shell-model configurations [61]. Obviously, the parameter P can describe such competition to an extent. Moreover, when each valence nucleon generally interacts with about 4–5 nucleons of the other type, namely, $P \approx 4$–5, the transition to deformation will take place. In Fig. 1(c), the P factors calculated by fixing $N_p = 10$ are shown for selected Hf isotopes. As expected, the $N = 104$ midshell nucleus ^{176}Hf with the largest number of valence neutrons has the maximum P value. Indeed, as shown in Fig. 1(a), the $R_{4/2}$ ratios reach the rotational limit ~ 3.3 near the $N = 104$ midshell, indicating the possible appearance of the maximum collectivity. Except for three lighter $^{156–160}$Hf nuclei, the P factors of other nuclei are all greater than 4, which means the onset of deformation. However, it should be noted that the shape transition point $R_{4/2} = 3.0$ corresponds to $P \approx 5.5$ instead of the empirical value ≈ 4–5, which can be easily understood since the exactly critical P point depends the relative integrated strengths of the p–n and like-nucleon-pairing interactions. Of course, the strengths of the corresponding p–n and pairing interactions are worth investigating in different isotopic chains in the future. In addition, by taking $N_p = \min[(Z - 50), (82 - Z)]$ and $N_n = \min[(N - 82), (126 - N)]$ [65], the symmetric contour map of the P factor is presented in Fig. 1(d) for even–even nuclei with $50 \leq Z \leq 82$ and $82 \leq N \leq 126$. If the empirical laws on the $R_{4/2}$ and P are accepted, combining these two contour maps of Figs. 1(b) and (d), one can to some extent provide further predictions for not only the unknown Hf isotopes but also the other unknown isotopes in this region.

As mentioned above, the phenomenological or empirical laws indicate that the selected Hf isotopes have large collectivity, namely, the deformed nuclear shape, which is usually described by the parametrization of the nuclear surface or the nucleon density distribution. In general, the multipole expansion of the nuclear surface with spherical harmonics is adopted in the phenomenological mean-field calculations (e.g., based on the WS potential), in which the shape degrees of freedom with low-order multipolarity will be considered to be of primary importance, e.g., β_2 deformation. As a basic test of the present model, Table 1 shows the calculated ground-state quadrupole deformation β_2 based on two sets of widely used WS parameters, which are simultaneously compared with several theoretical results and/or available data. The calculations used for evaluating the present results were performed based on the fold-Yukawa (FY) single-particle potential and the finite-range droplet model (FRDM) [66], the Hartree–Fock–BCS (HFBCS) [67], and the extended Thomas–Fermi plus Strutinsky integral (ETFSI) methods [68], respectively. The experimental β_2 value is deduced from the intrinsic quadrupole moment, which is related to the reduced electric quadrupole transition probability $B(E2)$ [69]. It is found in this table that the large collective behaviors have been reproduced in most nuclei though there is some difference among these values. One can clearly notice that the calculated quadrupole deformation β_2 is somewhat model- and parameter-dependent. All the theoretical calculations cannot completely reproduce the experimental data and agree with each other (especially for weakly deformed nuclei, e.g., $^{156–158}$Hf), but the general trend that they exhibit is similar. For instance, the β_2 deformations obtained both experimentally and theoretically will reach the maximum near the $N = 104$ midshell nucleus ^{176}Hf (halfway between the $N = 82$ and $N = 126$ major shell closures) and decrease as the neutron number N moves away from the midshell

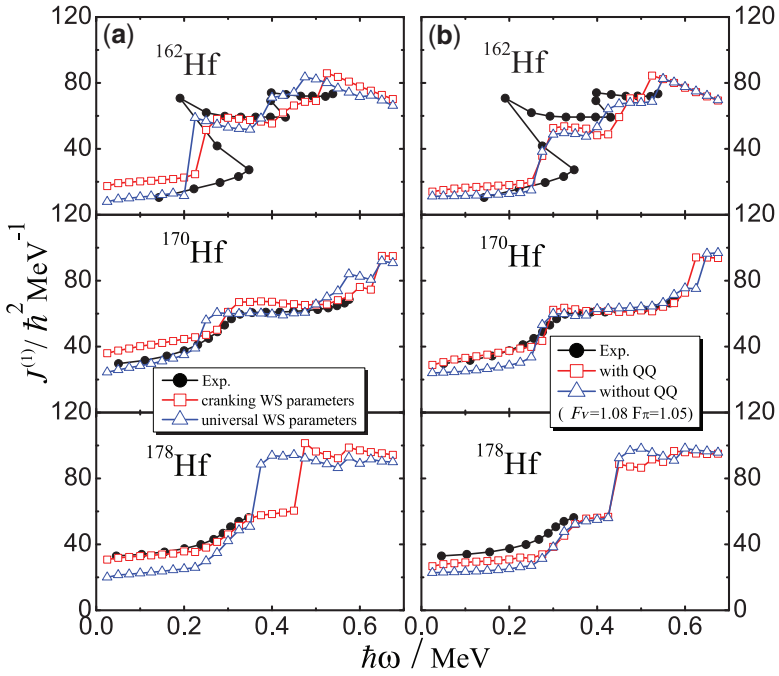

Fig. 2. (a) The kinematic moments of inertia $J^{(1)}$ calculated with universal WS parameters (open triangles) and cranking WS parameters (open squares) for three selected even–even nuclei ^{162,170,178}Hf, together with the available experimental data (filled circles) for comparison. (b) Similar to (a), but the TRS results are calculated based on cranking WS parameters and adjusted pairing strengths ($G = FG_0$). Moreover, as (b) shows, the open squares and triangles denote the calculations with and without the QQ pairing interaction, respectively.

number. Dudek et al. [70] analyzed the relationship between the WS potential parameters and the nucleonic distributions and suggested a corrected formula to modify the shape inconsistency. In addition, the effect of zero-point motion, which would imply that the experiment-comparable deformations are not static values but rather the most likely deformations calculated from the solutions of the collective motion, may be partly responsible for the existing difference between theory and experiment [71].

To investigate the nuclear properties under rotation, large collectivity (like in the present case) is favorable. Here it should be noted that the universal parameters are valid for describing the properties of the ground and high-K states [27], while the cranking parameters are more suitable for the rotational state (e.g., see Refs. [45,46] and references therein). As one of the important features, the kinematic moments of inertia $J^{(1)}$ calculated respectively by $J^{(1)} = I_x/\omega$ and $J^{(1)} = \hbar^2(2I-1)/E_\gamma(I \to I-2)$ theoretically and experimentally are shown in Fig. 2 for three arbitrarily selected ^{162,170,178}Hf nuclei. Figure 2(a) shows the results calculated with universal and cranking WS parameters, indicating that the calculated values with universal parameters are systematically lower than those of the cranking ones, at least before backbending. It seems that it is difficult to deduce which parameter set is better to describe the data. For instance, the universal parameters could give a more suitable description for ^{162}Hf, while the cranking parameters do so for ^{178}Hf. However, if the relative actual pairing interaction is considered (e.g., adjusting the pairing strength accordingly from the experimental mass data), the results calculated with the cranking parameters can actually agree with the data, as shown in Fig. 2(b). Thus, the following calculations for rotating nuclear properties are performed in terms of the cranking parameter set. Note that, for simplicity, the monopole pairing strength G_0 is

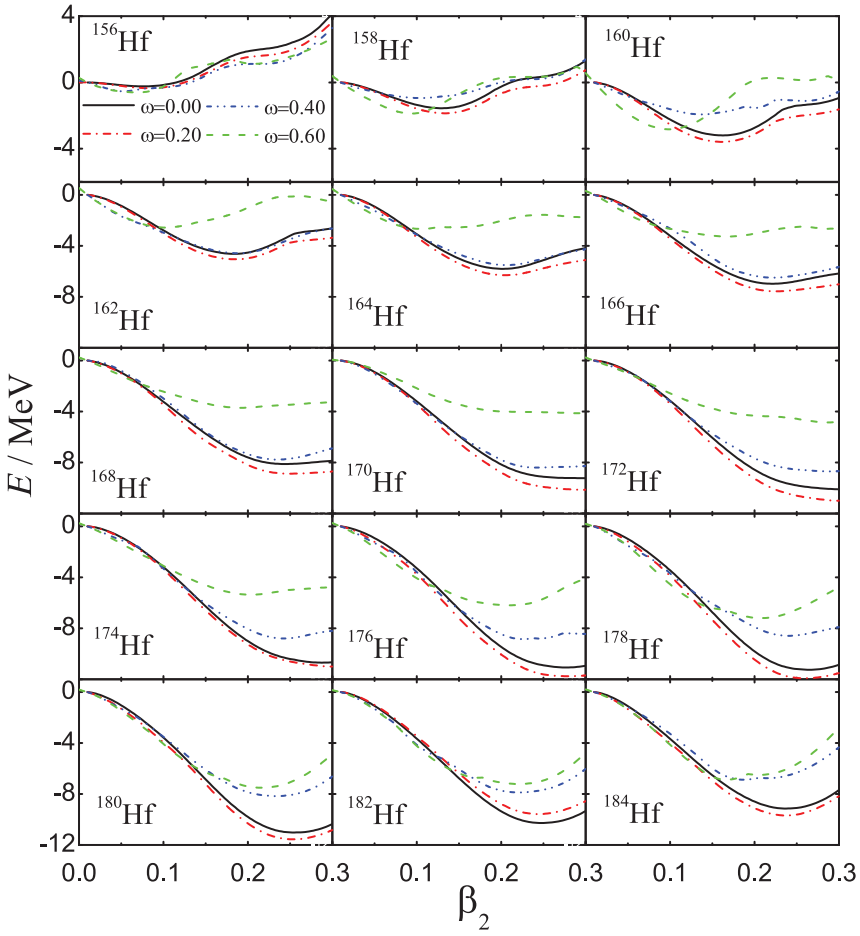

Fig. 3. Total deformation Routhian curves against β_2 for even–even $^{156-184}$Hf at several selected rotational frequencies ω = 0.00 (black solid), 0.20 (red dash-dotted), 0.40 (blue dash-dot-dotted), 0.60 (green dashed) MeV/$\hbar$. The energy (Routhian) has been minimized with respect to γ and β_4 at each (β_2, ω) point.

crudely adjusted according to the empirical values of this mass region suggested by Xu et al. [72]; e.g., the constant factors $F_\nu = 1.08$ for neutrons and $F_\pi = 1.05$ for protons are used. It can be seen, as expected, that the increase of the monopole pairing strength may decrease the moment of inertia and delay the backbending (or upbending) frequency due to the increasing superfluidity and broken-pair difficulty, respectively. Simultaneously, the effect of the quadrupole–quadrupole (QQ) pairing correlations on the moment of inertia is investigated by the calculations with and without the QQ pairing interaction. It is found that the existence of the QQ pairing force seems to increase the moment of inertia in the low-spin region but decrease the moment of inertia at high spin, e.g., after backbending. More detailed discussions of the influence of the QQ pairing on nuclei can be found in, e.g., Refs. [30,47,73,74].

It is well known that the nuclear mean-field (shape) and pairing interaction are actually two important factors affecting the moment of inertia. As seen in Table 1, one can see that the equilibrium shape, e.g., determined by minimizing the nuclear energy surface in a selected deformation space, depends rather on models and their parameters, especially for soft nuclei that have relatively flat energy surfaces. To gain a better understanding of nuclear shape and softness, Figs. 3 and 4 show the total Routhian curves along the minimum valley of the calculated TRS in the β_2 and γ directions,

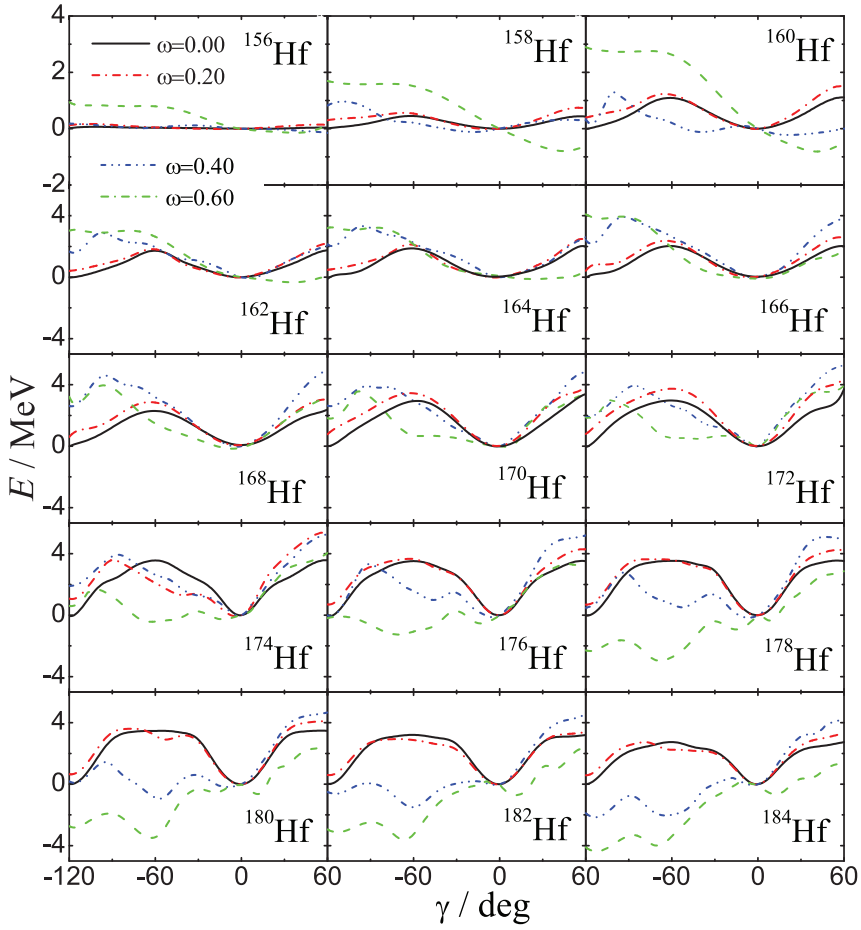

Fig. 4. Similar to Fig. 3, but against the γ deformation degree of freedom.

respectively, at four typical rotational frequencies. Such curves are relatively model- and parameter-independent, showing the evolution of shape and softness of nuclei with rotation. For example, Figs. 3 and 4 show that $^{164–174}$Hf (especially $^{168–172}$Hf) are relatively soft in both the β_2 and γ directions, indicating the possible occurrence of triaxial superdeformed structures, which is in good agreement with the results given in Refs. [75–78]. Figure 4 shows that the phenomena of prolate and oblate shape coexistence/transition occur in the heavier Hf nuclei at high spins, which is supported by previous work, e.g., in ^{180}Hf [79]. In ^{184}Hf, when the rotational frequency reaches 0.60 MeV/$\hbar$, the minimum appears at $\gamma \sim -120°$, corresponding to rotation around a prolate symmetry axis, which indicates that the yrast state at this moment will be of non-collective type (a similar situation occurs in W isotopes [80–83]). In addition, the flatness near the minimum of the deformation Routhian curve basically agrees with the facts of the observed β and/or γ vibration bands, e.g., in $^{168–180}$Hf [84–90].

Taking the evolution of nuclear shape and softness into account, one may well understand nuclear rotational properties. Now, similar to Fig. 2(a), Fig. 5 shows the kinematic moments of inertia $J^{(1)}$ calculated in terms of the cranking potential parameters for even–even $^{156–184}$Hf, together with the experimental results based on the available data for comparison. Apparently, the experimental backbending (or upbending) phenomena and the magnitudes in moments of inertia are well reproduced, at least in $^{158–178}$Hf, by the present calculations, except for ^{156}Hf and $^{180–184}$Hf, where the

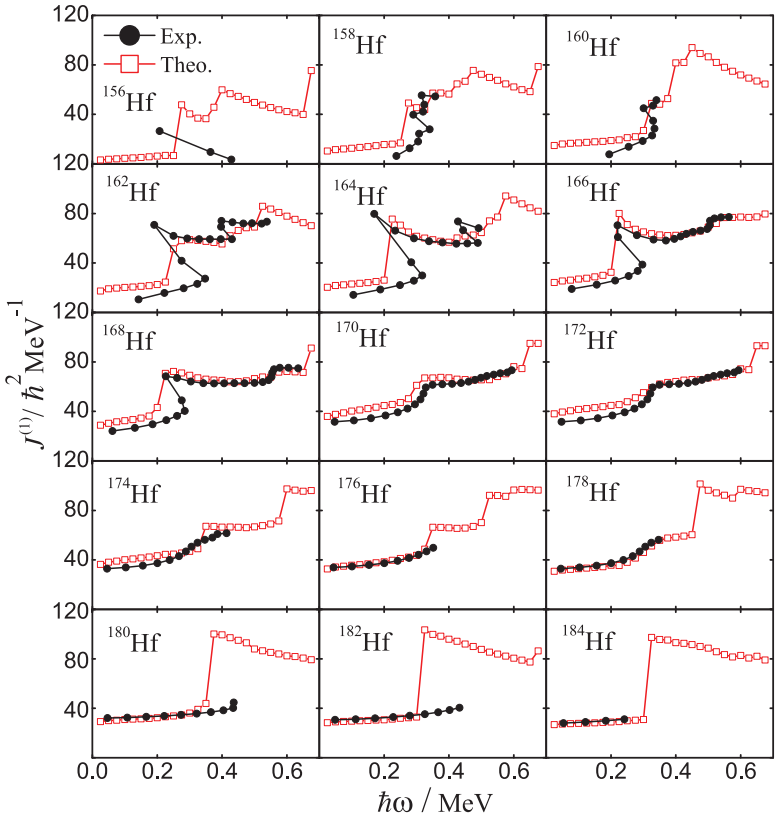

Fig. 5. The experimental (solid symbols) and predicted (open symbols) kinematic moments of inertia $J^{(1)}$ for even–even nuclei $^{156-184}$Hf as a function of rotational frequency. Note that the calculations are performed in terms of cranking WS parameters and with the inclusion of the QQ pairing interaction. The experimental data are taken from Refs. [79,88–100].

backbending (or upbending) frequencies cannot be deduced due to data scarcity. However, it seems that, especially in $^{180-182}$Hf, the calculated backbending points are obviously underestimated. Sometimes, the upbending phenomenon is observed instead of backbending due to the strong interaction between the ground-state band and rotation-aligned S band [4,96]. Note that the very limited energy levels in ^{156}Hf with $N = 84$ (close to the 82 magic number) have exhibited the single-particle excited property although, e.g., the $R_{4/2}$ ratio is almost on the so-called Mallmann critical point (see Fig. 1).

In order to understand the anomalies (backbending or upbending phenomena) and the magnitudes of the moments of inertia, which are related to the rotation alignments of nucleon pairs, especially those occupying the high-j orbitals near the Fermi surface, we display the calculated aligned angular momenta in Fig. 6, together with the proton and neutron components used to evaluate the rotation alignments of proton and/or neutron pairs. The general trend of the first anomaly shows that the proton rotation alignments seem to be favorable in the three lighter nuclei $^{156-160}$Hf, whereas the neutron alignments are favored in $^{162-178}$Hf; interestingly, for $^{180-184}$Hf, competition between the neutron and proton alignments occurs, indicating large aligned angular momenta (moment of inertia), which it would be desirable to confirm experimentally. The second yrast anomaly is attributable to a rotation-aligned neutron pair in $^{156-160}$Hf and proton pair, e.g., in ^{162,170}Hf, while in $^{174-178}$Hf such anomalies seem to appear due to competing proton and neutron alignments. Indeed, the alignments of the $i_{13/2}$ neutron pair and $h_{11/2}$ proton pair are generally

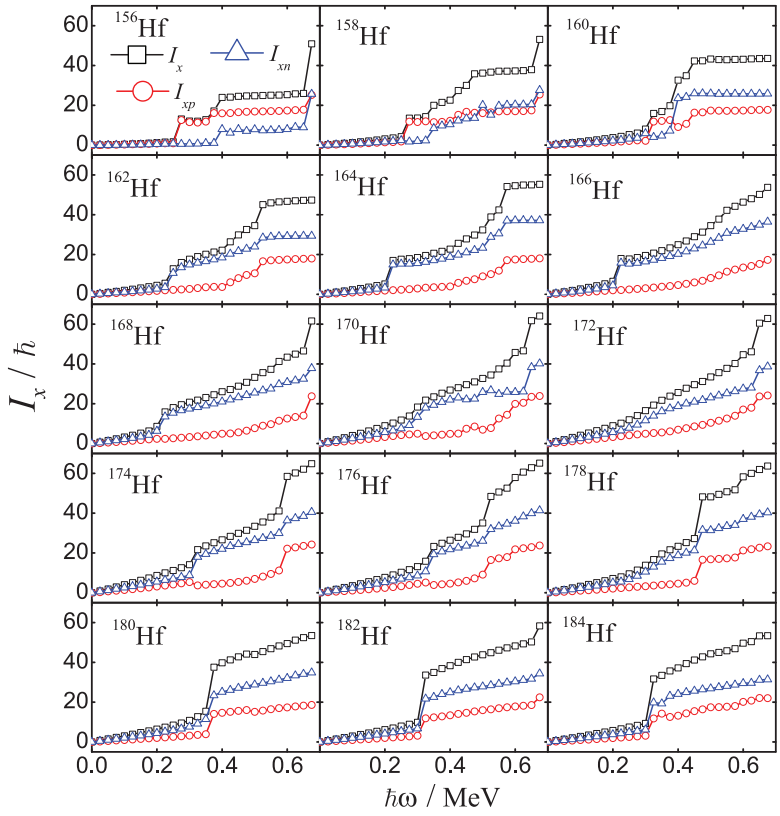

Fig. 6. The calculated aligned angular momentum I_x (squares) for even–even nuclei $^{156–184}$Hf as a function of rotational frequency. Proton I_{xp} (circles) and neutron I_{xn} (triangles) components are shown simultaneously.

pointed out to be respectively responsible for the first and second yrast anomalies in this deformed region [30,79,99,101,102].

In such regions, however, many distinct rotational bands up to a rather high-spin state (e.g., above 20$\hbar$) for a nucleus have been established, including different prolate, oblate, multi-quasiparticle, and even superdeformed bands. Some of these bands have energies (for a given spin) within a narrow domain of one another (e.g., five bands with energies for a fixed spin within 0.5 MeV in ^{174}Hf [99]), so that no one rotational band is strongly favored. It could be easily understood that at this moment such bands may cross one another at some rotational frequencies, which will produce a relatively complicated yrast structure. As shown in Fig. 5, the moments of inertia in both experiment and theory are actually hard to understand just based on the conventional framework, namely, the alignment of nucleon pairs. In particular, the so-called competition of proton and neutron alignments may be misunderstood when the aligned angular momenta of protons and neutrons dramatically increase at the same time. For instance, as shown in Fig. 6, the second obvious rise of aligned angular momentum in ^{174}Hf seems to originate from a simultaneous alignment of protons and neutrons, but the origin of such a rotational anomaly is the crossing of two bands with different deformations [99]. With this in mind, Fig. 7 shows the details of structure evolution along the yrast sequence in three selected $^{176–180}$Hf nuclei, representing different situations to an extent. Note that the present TRS calculation without configuration tracking could provide information on the yrast state well, though it will usually not be able to give non-yrast information except for the shape-coexisting configurations. From this figure, one can see these three sample nuclei undergo different structure evolution along their yrast lines, showing that most of the phenomena on the so-called double crossing (namely, the

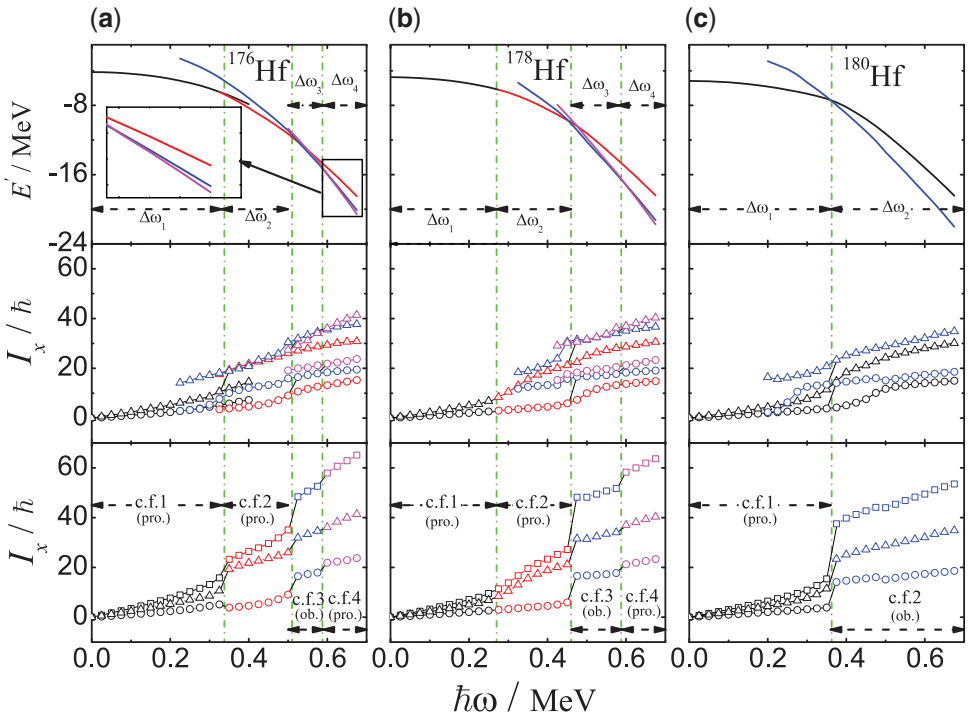

Fig. 7. (a) Top: total Routhians of the bands with different configurations (e.g., c.f.1, c.f.2, …) in ^{176}Hf as a function of rotational frequency. Middle: aligned angular momenta of protons (circles) and neutrons (triangles) for different shape-coexisting configurations in ^{176}Hf. Bottom: similar to Fig. 6; calculated aligned angular momenta, including proton (circles), neutron (triangles), and two combined (squares) ones, along the yrast sequences in ^{176}Hf. Different colors of total Routhians and aligned angular momenta indicate that these quantities come from the bands with different configurations. (b) and (c) are similar to (a) but for ^{178}Hf and ^{180}Hf, respectively.

simultaneous alignments of protons and neutrons) usually come from a shape jump. In Fig. 8, detailed calculations show that the shape transitions from prolate ($\gamma \sim 0°$) to oblate ($\gamma \sim$ -60°) take place along the yrast lines in the lighter $^{156–160}$Hf and heavier $^{176–184}$Hf nuclei (even non-collective oblate configurations appear in $^{156–160}$Hf). A more detailed configuration analysis for each component along the yrast line in principle needs configuration-controlled TRS calculations, which are beyond the scope of this work.

3.2. Analysis of novel E-GOS curves

To gain a better understanding of the collectivity evolution (including the difference in the moment of inertia between theory and experiment) along the yrast line, we may have to consider different motion modes and their coupling (e.g., due to the soft deformation Routhian curves in some nuclei, as shown in Figs. 3 and 4), though the present model cannot include such mechanisms. Regan et al. [103] have proposed an empirical E-GOS (E-gamma over spin; namely, a function $R(I) = E_\gamma(I \to I-2)/I$) curve to manifest the shape/phase transition between vibration and rotation along the yrast line. In the ideal situation, the $R(I)$ functions can be derived to be $E_\gamma(2 \to 0)/I$, $E_\gamma(2 \to 0)[1/4 + 1/(2I)]$, and $E_\gamma(2 \to 0)[2/3 - 1/(3I)]$ based on the energy formulas $E(I) \propto I$, $I(I+6)$, and $I(I+1)$ for a vibrator, a γ-soft rotor, and an axially symmetric rotor, respectively. As given by Regan et al. [103], based on the energies $E(2^+)$ of the typical first 2^+ excited states, Fig. 9(a) shows the corresponding

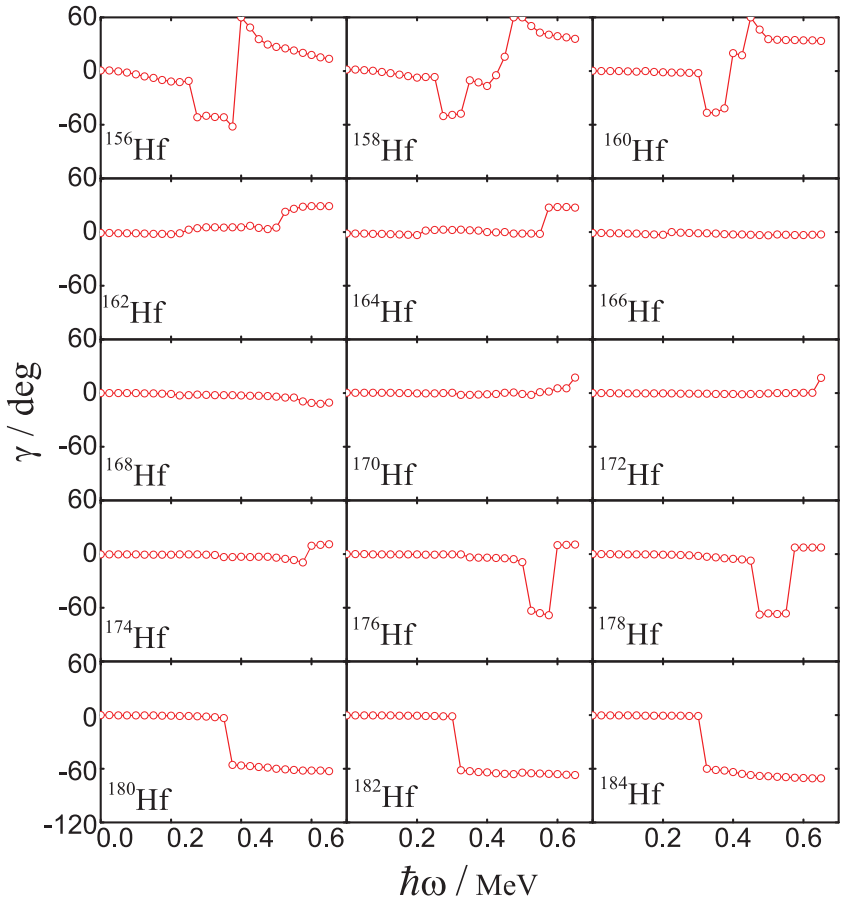

Fig. 8. The calculated γ deformation for even–even nuclei $^{156-184}$Hf as a function of rotational frequency.

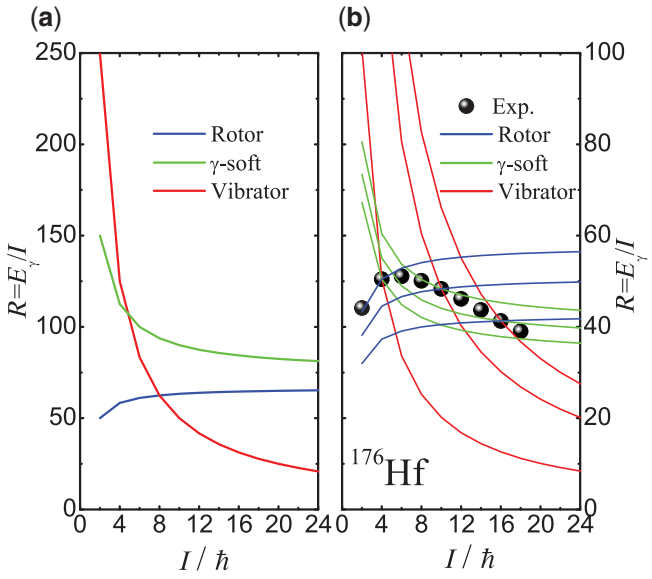

Fig. 9. (a) Typical E-GOS curves for a perfect harmonic vibrator, γ-soft, and axially symmetric rotors with the first 2^+ excitations of 500, 300, and 100 keV, respectively [103]. (b) Similar to (a); three sets of such E-GOS curves at the selected spins $I = 4$, 12, and $16\hbar$, together with the experimental data (filled circles) for ^{176}Hf. Note that, at each selected spin point, the red, green, and blue lines denote the E-GOS curves with vibrational, γ -soft, and rotational modes, respectively.

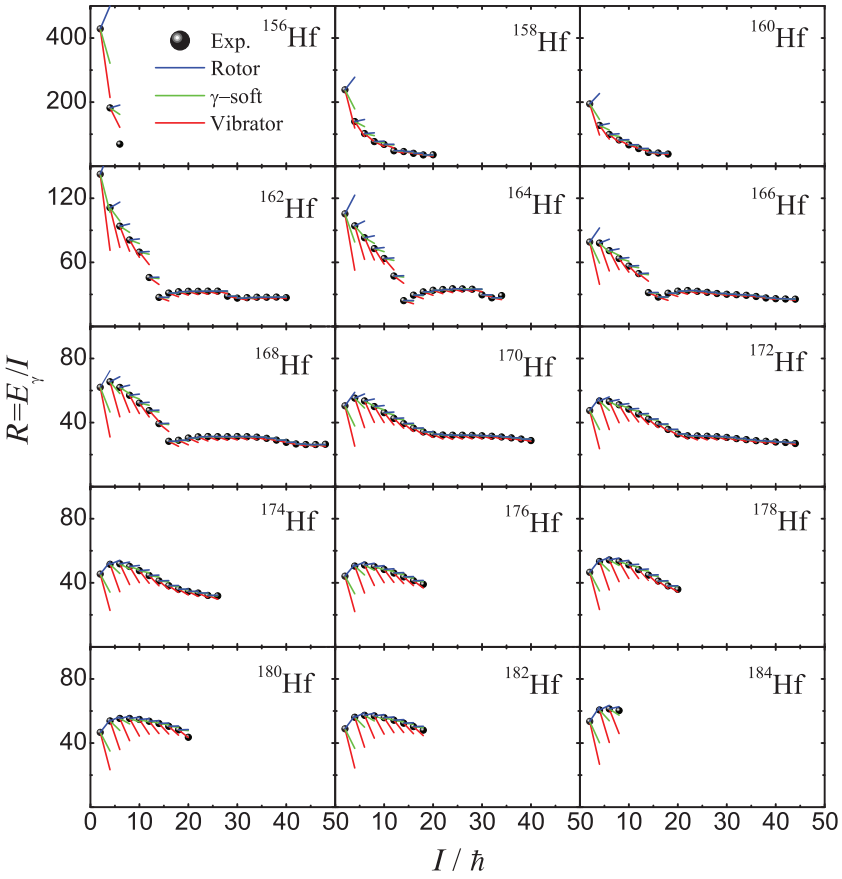

Fig. 10. Similar to Fig. 9(b); the centipede-like E-GOS curves along the yrast sequences for even–even $^{156-184}$Hf isotopes.

E-GOS curves. More generally, inspired by this idea, one can give a set of corresponding E-GOS curves according to each selected $E^s_\gamma(I^s \to I^s - 2)$ energy observed experimentally. That is, now the corresponding $R(I)$ ratios will respectively obey the function relationships $E^s_\gamma(I^s \to I^s - 2)/I$, $[E^s_\gamma(I^s \to I^s - 2)/(I^s + 2)](1 + 2/I)$, and $[E^s_\gamma(I^s \to I^s - 2)/(2I^s - 1)](2 - 1/I)$ for a vibrator, a γ-soft rotor, and an axially symmetric rotor. Therefore, at each spin we can, in principle, plot a set of E-GOS curves that pass the $R(I^s)$ point. Typically, the curve for the axially rigid rotor has an opposite changing (increasing) trend relative to the other two cases. Figure 9(b) shows three such sets of E-GOS curves based on low, medial, and high spin-point $E^s_\gamma(I^s \to I^s - 2)$ rays for ^{176}Hf. Obviously, if one of the assumed motion modes (vibration, γ-soft, and rigid rotor) is reasonable, the adjacent point except for the band-crossing one will usually fall on the corresponding E-GOS curve since the adjacent points have the greatest possibility with the same excitation modes. In order to clearly display the evolution of different motion modes, we suggested a new centipede-like E-GOS curve [34,35], in which three corresponding curves were cut off and just the parts from one $R(I)$ to its next adjacent $R(I + 2)$ point were kept. Figure 10 shows such centipede-like E-GOS curves along the yrast sequences for even–even $^{156-184}$Hf isotopes. It can be seen that none of the yrast bands exhibits one pure motion mode. In the lighter nuclei $^{156-166}$Hf, there is an evolution picture from vibration (or γ-soft) to rotation, while there seems to be a trend from rotation to vibration (or γ-soft) for $^{168-184}$Hf. Similar evolution properties were discussed in previous works [103,104].

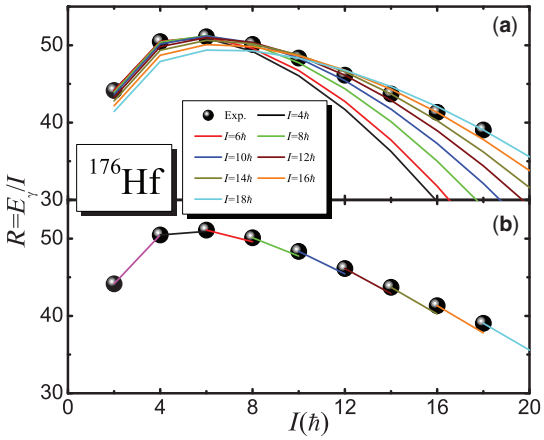

Fig. 11. (a) E-GOS curves including a first-order rotation–vibration interaction [52] for ^{176}Hf. The curves with different colors indicate that they cross the corresponding $R(I)$ data. (b) The improved E-GOS curve constituted by the $R(I) \rightarrow R(I+2)$ line segments.

If the first-order rotation–vibration interaction [52,105] is taken into account, the energy expression of a rotational state with angular momentum I in an axially symmetric nucleus is usually written as $E(I) = AI(I+1)+B[I(I+1)]^2$, where A and B are constants. In principle, the high-order correction $B[I(I+1)]^2$ term can be from many effects [106], e.g., the rotation–vibration coupling [52,105] and pairing correlation correction [107]. Similar to Refs. [52,105], we temporarily suppose that this term is related to the first-order rotation–vibration coupling and further extend the E-GOS curve by using this energy formula, aiming to investigate to what extent the predicted evolution trend can be improved. As done above, based on a simple derivation, the $R(I)$ in this situation will be $f(I)(2-1/I)$ and the spin-dependent factor $f(I)$ equals $2A+2B[I(I+1)+(I-2)(I-1)]$. Of course, one can easily get the constants A and B from two arbitrarily selected and adjacent energy levels $E^s(I^s)$ and $E^s(I^s-2)$ or γ rays $E^s_\gamma(I^s \rightarrow I^s-2)$ and $E^s_\gamma(I^s-2 \rightarrow I^s-4)$. Therefore, from the second spin point $I = 4\hbar$, the new E-GOS curve passing the corresponding experimental point $R(I^s)$ can be plotted for the selected ^{176}Hf nucleus, as shown in Fig. 11(a). Compared with the E-GOS curves in Fig. 9(b) where the pure motion mode is assumed, the new curve with the inclusion of the first-order rotation–vibration interaction obviously describes the data better, though there is still no one curve that passes all the data. As mentioned above, if the reasonable assumption that adjacent levels have similar excited modes is considered, the improved centipede-like E-GOS curve can be obtained after each $R(I^s) \rightarrow R(I^s+2)$ line segment is retained, as shown in Fig. 11(b). It seems that such a development is interesting. However, it is worth noting that the energy formula $E(I) = AI(I+1)+B[I(I+1)]^2$ with a first-order rotation–vibration approximation is suitable for relatively well deformed nuclei, e.g., with the ratio $R_{4/2} > 8/3$ [52]. Thus, taking the $R_{4/2}$ values in Fig. 1(a) as a reference, we select even–even nuclei $^{168-184}$Hf to test the present development on the E-GOS curve, as shown in Fig. 12. Indeed, one can find that the description of the data is improved to a large extent, which means that the vibration effect is of importance in well deformed nuclei as well as weakly deformed soft nuclei under rotation. Based on such a test, a further theoretical development certainly seems to be necessary in our future work, including consideration of the effect from the different high-order correction components.

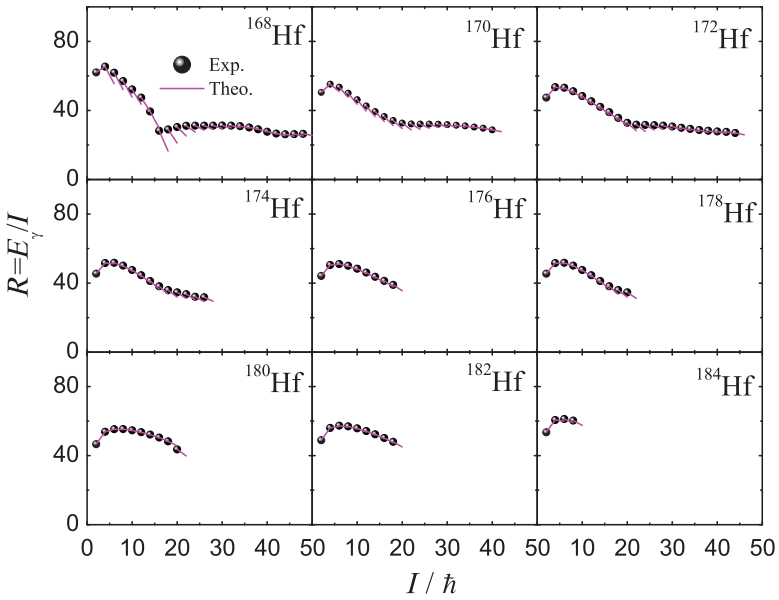

Fig. 12. Similar to Fig. 11; the improved E-GOS curves along the yrast sequences for even–even $^{168–184}$Hf isotopes with $R_{4/2} > 8/3$ where the rotation–vibration interaction could be approximately adopted.

4. Summary

In summary, the evolution of collectivity along the yrast sequence for even–even $^{156–184}$Hf nuclei has been systematically investigated in terms of deformation-pairing self-consistent calculations. As a basic model test, calculated ground-state deformations are compared with other theoretical results and available experimental data, showing a satisfactory agreement. Based on the deformation Routhian curves at different rotational frequencies, nuclear shape and softness evolution with rotation are evaluated. The soft energy surfaces are in good agreement with the facts observed for the γ and/or β vibrational bands. The observed backbending (or upbending) in moments of inertia are well reproduced theoretically and the reasons for the existing difference between experiment and theory are analyzed from various aspects (e.g., shape, pairing, and the coupling of different motion modes). The aligned angular momenta including proton and neutron components are calculated to show the possible mechanism of backbending (or upbending). It is found that most of the simultaneous alignments of protons and neutrons may be attributable to a large shape change (jump) rather than the double band-crossing (namely, the so-called competition of proton and neutron alignments). The centipede-like E-GOS curves are used to understand the evolution of nuclear collectivity, indicating a non-ignorable vibration effect. Moreover, taking the first-order rotation–vibration interaction into account, we further extend the centipede-like E-GOS curve, which can actually agree with the expected trend. The present work provides a helpful understanding of the yrast structures for Hf isotopes (especially for the high-isospin nuclei and/or high-spin region due to data scarcity) by using macroscopic–microscopic calculations and further arranges (or extends) the empirical laws (e.g., summarizing the eight critical $R_{4/2}$ values and extending the E-GOS curve), which are usually simple but very valid for understanding nuclear collectivity and its evolution, including model testing and development.

Acknowledgements

This work is supported by the Natural Science Foundation of China (Grant Nos. 11675148), the Project of Youth Backbone Teachers of Colleges and Universities of Henan Province (No. 2017GGJS008), the Outstanding

Young Talent Research Fund of Zhengzhou University (Grant No. 1521317002), the Physics Research and Development Program of Zhengzhou University (Grant No. 32410017), and the Foundation and Advanced Technology Research Program of Henan Province (Grant No. 162300410222).

References

[1] B. Bastin et al., Phys. Rev. Lett. **99**, 022503 (2007).
[2] A. Obertelli et al., Phys. Lett. B **633**, 33 (2006).
[3] K. G. Wilson, Rev. Mod. Phys. **55**, 583 (1983).
[4] A. Johnson, H. Ryde, and J. Sztarkier, Phys. Lett. B **34**, 605 (1971).
[5] M. Bender, P.-H. Heenen, and P.-G. Reinhard, Rev. Mod. Phys. **75**, 121 (2003).
[6] S. C. Pieper, K. Varga, and R. B. Wiringa, Phys. Rev. C **66**, 044310 (2002).
[7] P. Navrátil, S. Quaglioni, I. Stetcu, and B. R. Barrett, J. Phys. G: Nucl. Part. Phys. **36**, 083101 (2009).
[8] L. S. Cardman, Eur. Phys. J. A **28**, 7 (2006).
[9] P. Cejnar, J. Jolie, and R. F. Casten, Rev. Mod. Phys. **82**, 2155 (2010).
[10] S. Goriely, N. Chamel, and J. M. Pearson, Phys. Rev. Lett. **102**, 152503 (2009).
[11] S. Goriely, S. Hilaire, M. Girod, and S. Péru, Phys. Rev. Lett. **102**, 242501 (2009).
[12] M. Rufa, P.-G. Reinhard, J. A. Maruhn, W. Greiner, and M. R. Strayer, Phys. Rev. C **38**, 390 (1988).
[13] P.-G. Reinhard, Rep. Prog. Phys. **52**, 439 (1989).
[14] W. D. Myers and W. J. Swiatecki, Nucl. Phys. **81**, 1 (1966).
[15] P. Möller, W. D. Myers, W. J. Swiatecki, and J. Treiner, At. Data Nucl. Data Tables **39**, 225 (1988).
[16] K. Pomorski and J. Dudek, Phys. Rev. C **67**, 044316 (2003).
[17] W. J. Swiatecki, Phys. Rev. **104**, 993 (1956).
[18] S. Cohen and W. J. Swiatecki, Ann. Phys. **22**, 406 (1963).
[19] D. R. Inglis, Phys. Rev. **96**, 1059 (1954).
[20] D. R. Inglis, Phys. Rev. **103**, 1786 (1956).
[21] J. R. Grover, Phys. Rev. **127**, 2142 (1962).
[22] M. J. A. de Voigt, J. Dudek, and Z. Szymański, Rev. Mod. Phys. **55**, 949 (1983).
[23] J. L. Gross and M. Thoennessen, At. Data Nucl. Data Tables **98**, 983 (2012).
[24] S. Goriely, M. Samyn, and J. M. Pearson, Phys. Rev. C **75**, 064312 (2007).
[25] M. Thoennessen, Rep. Prog. Phys. **67**, 1187 (2004).
[26] G. A. Souliotis, Phys. Scripta **T88**, 153 (2000).
[27] F. R. Xu, P. M. Walker, J. A. Sheikh, and R. Wyss, Phys. Lett. B **435**, 257 (1998).
[28] W. Nazarewicz, R. Wyss, and A. Johnson, Nucl. Phys. A **503**, 285 (1989).
[29] W. Satuła, R. Wyss, and P. Magierski, Nucl. Phys. A **578**, 45 (1994).
[30] F. R. Xu, P. M. Walker, and R. Wyss, Phys. Rev. C **62**, 014301 (2000).
[31] H. C. Pradhan, Y. Nogami, and J. Law, Nucl. Phys. A **201**, 357 (1973).
[32] H.-L. Wang, J. Yang, M.-L. Liu, and F.-R. Xu, Phys. Rev. C **92**, 024303 (2015).
[33] H.-L. Wang, S. Zhang, M.-L. Liu, and F.-R. Xu, Prog. Theor. Exp. Phys. **2015**, 073D03 (2015).
[34] Q. Yang, H.-L. Wang, M.-L. Liu, and F.-R. Xu, Phys. Rev. C **94**, 024310 (2016).
[35] J. Yang, H.-L. Wang, Q.-Z. Chai, M.-L. Liu, and F.-R. Xu, Prog. Theor. Exp. Phys. **2016**, 063D03 (2016).
[36] V. M. Strutinsky, Nucl. Phys. A **95**, 420 (1967).
[37] S. Cwiok, J. Dudek, W. Nazarewicz, J. Skalski, and T. Werner, Comp. Phys. Commun. **46**, 379 (1987).
[38] W. Nazarewicz, J. Dudek, R. Bengtsson, T. Bengtsson, and I. Ragnarsson, Nucl. Phys. A **435**, 397 (1985).
[39] P. Möller and J. R. Nix, Nucl. Phys. A **536**, 20 (1992).
[40] W. Satuła and R. Wyss, Phys. Rev. C **50**, 2888 (1994).
[41] R. Bengtsson, S. E. Larsson, G. Leander, P. Möller, S. G. Nilsson, S. Åberg, and Z. Szymański, Phys. Lett. B **57**, 301 (1975).
[42] K. Neergård and V. V. Pashkevich, Phys. Lett. B **59**, 218 (1975).
[43] K. Neergård, V. V. Pashkevich, and S. Frauendorf, Nucl. Phys. A **262**, 61 (1976).
[44] G. Andersson et al., Nucl. Phys. A **268**, 205 (1976).
[45] A. Bhagwat, X. Viñas, M. Centelles, P. Schuck, and R. Wyss, Phys. Rev. C **81**, 044321 (2010).
[46] W. Satuła and R. A. Wyss, Rep. Prog. Phys. **68**, 131 (2005).
[47] W. Satuła and R. Wyss, Phys. Scripta **T56**, 159 (1995).

[48] H. Sakamoto and T. Kishimoto, Phys. Lett. B **245**, 321 (1990).
[49] F. R. Xu, W. Satuła, and R. Wyss, Nucl. Phys. A **669**, 119 (2000).
[50] P. Ring, R. Beck, and H. J. Mang, Z. Phys. **231**, 10 (1970).
[51] A. Bohr, Dan. Mat. Fys. Medd. **26**, 1 (1952).
[52] C. A. Mallmann, Phys. Rev. Lett. **2**, 507 (1959).
[53] J. B. Gupta, Int. J. Mod. Phys. E **22**, 1350023 (2013).
[54] F. Iachello, Phys. Rev. Lett. **87**, 052502 (2001).
[55] D. Bonatsos, D. Lenis, D. Petrellis, and P. A. Terziev, Phys. Lett. B **588**, 172 (2004).
[56] M. A. J. Mariscotti, Phys. Rev. Lett. **24**, 1242 (1970).
[57] A. S. Davydov and G. F. Filippov, Nucl. Phys. **8**, 237 (1958).
[58] F. Iachello, N. V. Zamfir, and R. F. Casten, Phys. Rev. Lett. **81**, 1191 (1998).
[59] R. F. Casten, D. Kusnezov, and N. V. Zamfir, Phys. Rev. Lett. **82**, 5000 (1999).
[60] N. Fouladi, J. Fouladi, and H. Sabri, Eur. Phys. J. Plus **130**, 112 (2015).
[61] R. F. Casten, D. S. Brenner, and P. E. Haustein, Phys. Rev. Lett. **58**, 658 (1987).
[62] R. F. Casten, Phys. Rev. Lett. **54**, 1991 (1985).
[63] R. F. Casten, Nucl. Phys. A **443**, 1 (1985).
[64] R. F. Casten and N. V. Zamfir, J. Phys. G: Nucl. Part. Phys. **22**, 1521 (1996).
[65] E. C. Halbert and W. Nazarewicz, Phys. Rev. C **48**, R2158(R) (1993).
[66] P. Moller, J. R. Nix, W. D. Myers, and W. J. Swiatecki, At. Data Nucl. Data Tables **59**, 185 (1995).
[67] S. Goriely, F. Tondeur, and J. M. Pearson, At. Data Nucl. Data Tables **77**, 311 (2001).
[68] Y. Aboussir, J. M. Pearson, A. K. Dutta, and F. Tondeur, At. Data Nucl. Data Tables **61**, 127 (1995).
[69] S. Raman, C. W. Nestor, and P. Tikkanen, At. Data Nucl. Data Tables **78**, 1 (2001).
[70] J. Dudek, W. Nazarewicz, and P. Olanders, Nucl. Phys. A **420**, 285 (1984).
[71] K. Mazurek, J. Dudek, A. Maj, and D. Rouvel, Phys. Rev. C **91**, 034301 (2015).
[72] F. R. Xu, R. Wyss, and P. M. Walker, Phys. Rev. C **60**, 051301(R) (1999).
[73] M. Wakai and A. Faessler, Nucl. Phys. A **295**, 86 (1978).
[74] M. Diebel, Nucl. Phys. A **419**, 221 (1984).
[75] A. Neußer-Neffgen et al., Phys. Rev. C **73**, 034309 (2006).
[76] D. J. Hartley et al., Phys. Lett. B **608**, 31 (2005).
[77] H. Amro et al., Phys. Lett. B **506**, 39 (2001).
[78] S. Mukhopadhyay et al., Phys. Rev. C **83**, 044311 (2011).
[79] U. S. Tandel et al., Phys. Rev. Lett. **101**, 182503 (2008).
[80] C. F. Jiao, Y. Shi, F. R. Xu, Y. Sun, and P. M. Walker, Sci. China G **55**, 1613 (2012).
[81] P. M. Walker and F. R. Xu, Phys. Lett. B **635**, 286 (2006).
[82] P. D. Stevenson, M. P. Brine, Zs. Podolyak, P. H. Regan, P. M. Walker, and J. Rikovska Stone, Phys. Rev. C **72**, 047303 (2005).
[83] K. Nomura, T. Otsuka, R. Rodríguez-Guzmán, L. M. Robledo, P. Sarriguren, P. H. Regan, P. D. Stevenson, and Zs. Podolyák, Phys. Rev. C **83**, 054303 (2011).
[84] C. M. Baglin, Nucl. Data Sheets **111**, 1807 (2010).
[85] C. M. Baglin, Nucl. Data Sheets **96**, 611 (2002).
[86] B. Singh, Nucl. Data Sheets **75**, 199 (1995).
[87] E. Browne and H. Junde, Nucl. Data Sheets **87**, 15 (1999).
[88] M. S. Basunia, Nucl. Data Sheets **107**, 791 (2006).
[89] A. B. Hayes et al., Phys. Rev. Lett. **89**, 242501 (2002).
[90] E. Ngijoi-Yogo et al., Phys. Rev. C **75**, 034305 (2007).
[91] D. Seweryniak et al., Phys. Rev. C **71**, 054319 (2005).
[92] K. Y. Ding et al., Phys. Rev. C **62**, 034316 (2000).
[93] H. Hübel, M. Murzel, E. M. Beck, H. Kluge, A. Kuhnert, K. H. Maier, J. C. Bacelar, M. A. Deleplanque, R. M. Diamond, and F. S. Stephens, Z. Phys. A **329**, 289 (1988).
[94] B. Singh, Nucl. Data Sheets **93**, 243 (2001).
[95] D. Ringkjøbing Jensen et al., Eur. Phys. J. A **8**, 165 (2000).
[96] R. Chapman et al., Phys. Rev. Lett. **51**, 2265 (1983).
[97] J. C. Lisle, J. D. Garrett, G. B. Hagemann, B. Herskind, and S. Ogaza, Nucl. Phys. A **366**, 281 (1981).
[98] E. S. Paul, R. Chapman, J. C. Lisle, J. N. Mo, S. Sergiwa, J. C. Willmott, and A. Holm, J. Phys. G: Nucl. Phys. **11**, L53 (1985).
[99] P. M. Walker et al., Phys. Lett. B **168**, 326 (1986).

[100] C. M. Baglin, Nucl. Data Sheets **111**, 275 (2010).
[101] F. S. Stephens and R. S. Simon, Nucl. Phys. A **183**, 257 (1972).
[102] R. Holzmann, J. Kuzminski, M. Loiselet, M. A. Van Hove, and J. Vervier, Phys. Rev. Lett. **50**, 1834 (1983).
[103] P. H. Regan et al., Phys. Rev. Lett. **90**, 152502 (2003).
[104] S. F. Shen, Y. B. Chen, F. R. Xu, S. J. Zheng, B. Tang, and T. D. Wen, Phys. Rev. C **75**, 047304 (2007).
[105] K. Alder, A. Bohr, T. Huus, B. Mottelson, and A. Winther, Rev. Mod. Phys. **28**, 432 (1956).
[106] A. Bohr and B. R. Mottelson, *Nuclear Structure* (Singapore, World Scientific, 1998), Vol. 2, p. 23.
[107] A. Faessler, W. Greiner, and R. K. Sheline, Nucl. Phys. **70**, 33 (1965).